Quantum paraelectricity in the H-bonded ferroelectrics KH_2PO_4 and KD_2PO_4 under pressure

F. Torresi,[1] J. Lasave,[1] E. Tosatti,[2,3] J. Kohanoff,[4] and S. Koval[1]
[1)] *Instituto de Física Rosario, Universidad Nacional de Rosario and CONICET, 27 de Febrero 210 Bis, 2000 Rosario, Argentina*
[2)] *SISSA, via Bonomea 265, I-34136 Trieste, Italy*
[3)] *ICTP, Strada Costiera 11, I-34014 Trieste, Italy*
[4)] *Instituto de Fusión Nuclear "Guillermo Velarde", Universidad Politécnica de Madrid, Calle de José Gutierrez Abascal 2, 28006 Madrid, Spain*

(*Electronic mail: koval@ifir-conicet.gov.ar)

(Dated: September 10, 2025)

By means of path integral Monte Carlo simulations based on a coarse-grained model parameterized by first-principles calculations, we reproduce the large isotope effect observed in H-bonded KH_2PO_4 (KDP) and deuterated DKDP, showing that the dramatic shift in the ferroelectric critical temperature T_c upon deuteration is governed by the effective mass and local geometry of hydrogen bonds. We find clear evidence of a quantum paraelectric (QPE) phase in KDP-type ferroelectrics at high pressures, characterized by a universal critical proton off-centering parameter (δ_c), independent of isotopic substitution. Remarkably, this universality explains the experimentally observed collapse of the isotope effect under pressure, reinforcing the essential role of geometrical effects. Our results suggest that the emergence of quantum paraelectricity and the universal linear behavior of T_c with δ across chemically diverse systems share a common microscopic origin associated with local proton delocalization within the hydrogen bond network.

PACS numbers: 77.84.Fa, 77.80.-e

I. INTRODUCTION

Quantum paraelectricity is an important topic in the field of ferroelectricity, particularly in the study of quantum phase transitions and critical phenomena. It is central to understanding materials where quantum fluctuations suppress ferroelectric (FE) order, stabilizing the soft mode. A prime example is strontium titanate ($SrTiO_3$), which remains paraelectric (PE) down to the lowest temperatures due to quantum fluctuations, despite exhibiting a soft phonon mode indicative of a ferroelectric instability[1]. This behavior has been extensively studied since the 1960s and continues to be a benchmark for quantum paraelectricity[2–7]. Theoretical frameworks, such as those developed by Rowley et al.[8], and experiments[9] have shown that tuning parameters like pressure or chemical composition can drive compounds through a quantum phase transition between FE and quantum paraelectric (QPE) states, with implications for developing novel functional materials and devices. Recent research has also demonstrated the ability to induce ferroelectricity in $SrTiO_3$ with terahertz fields, showcasing the dynamic control over phase transitions in QPE materials[10].

Interestingly, growing evidence suggests that similar quantum paraelectric behavior may also emerge in hydrogen-bonded ferroelectrics under specific conditions such as high pressure or isotopic substitution[11–15]. A notable case is potassium dihydrogen phosphate (KH_2PO_4, KDP), which is the prototypical members of a broad class of hydrogen-bonded ferroelectrics, where ferroelectricity arises from the off-center proton ordering along H-bonds that link phosphate units[16] (see Fig. 1a)). In the PE phase at high temperature, the H atoms statistically occupy, with equal probability, two symmetric positions along the H-bond, separated a distance δ which characterizes the disordered phase[11]. Below T_c the protons localize into one of the symmetric sites, leading to the ordered FE phase[17]. The FE transition in KDP is characterized as weakly first order[18]. The transition rapidly becomes second order under pressure, with a tricritical pressure of ≈ 2.7 kbar[19,20].

Beyond its well-known applications in nonlinear optics as a harmonic generator and parametric oscillator, KDP is also used as an agricultural plant nutrient and a buffering agent for pharmaceutical products. However, from the fundamental point of view, KDP has attracted much attention due to its huge isotope effect, where the ferroelectric critical temperature T_c shifts from $\approx$ 122K in KDP to $\approx$ 229K in its deuterated counterpart (DKDP). Despite having been extensively studied, the underlying origin of this remarkable isotope effect remains a subject of ongoing debate[21]. Early attempts to explain this phenomenon invoked a famous tunneling model in the 1960s[22], while later neutron diffraction studies in the 1990s emphasized the importance of geometrical effects[11,23], namely the modification of hydrogen bonds by isotope substitution, known as the geometric or Ubbelohde effect[24], which manifests as larger δ and O–O distances upon deuteration[17,25]. Specifically, neutron diffraction studies further showed that T_c appears linearly correlated with the mean H off-center displacement $x \equiv \delta/2$, and is predicted to vanish under high pressure, suggesting the possible emergence of a quan-

tum paraelectric state[11,23].

That is indeed the case but, quite surprisingly, it appears to be independent of isotopic substitution. Neutron diffraction experiments under pressure show that the observed T_c vs. δ behaviors of KDP and DKDP coincide within error bars. As pressure increases both compounds approach the same critical value $\delta_c \approx 0.22$ Å[11], below which T_c vanishes and the FE phase disappears. Even more striking is that other H-bonded FE and antiFE compounds like lead hydrogen phosphate (LHP) and squaric acid (H2SQ) also exhibit a similar pressure evolution and share with KDP and DKDP the same δ_c. This critical magnitude therefore seems to be universal, independent of the chemical environment[11] (see Fig. 6). The H-bond networks in LHP, H2SQ, and KDP have, respectively, one-, two-, and three-dimensional character, so this universal behavior appears also to be independent of dimensionality. Compton scattering, at the same time, clearly shows the demise of deuteron tunneling in DKDP[26] as opposed to pronounced proton tunneling in KDP.[27] First-principles (FP) calculations further suggested that the large isotope effect is driven by a complex self-consistent interplay between tunneling and H-bond geometric effects, (specifically H-bond length and the related crystal volume), each amplifying the other[16,17]. In spite of all the progress made in the past decades, a detailed description and understanding of the quantum phase transition, of related isotope and geometric effects, as well as the possible existence of a QPE state under pressure is still lacking. Here, we focus explicitly on the pressure-induced emergence of quantum paraelectricity, its microscopic origin, and its relationship to geometric effects in the phase transitions of KDP and DKDP.

Over the years, numerous phenomenological models have been proposed to explore isotope effects in H-bonded ferroelectric materials[28–31], mostly parameterized with experimental data. Some of us proposed a simple self-consistent model parameterized on the basis of reliable FP calculations that shed light into the microscopic behavior of KDP and DKDP[16]. This model, which contained a single degree of freedom (x, defined above) with an effective mass, allowed for the incorporation of quantum nuclear effects and for scrutinizing the interplay between tunneling and geometric effects. In its simplicity, the model lacked interactions with neighboring degrees of freedom and thus it could not be used to study phase transitions. In addition, it did not include coupling to strain, essential to study the behavior under pressure. Further FP calculations using more advanced functionals in DFT, served to refine the various model parameters[32]. In parallel, thermal and quantum nuclear effects were taken into account via first-principles path-integral (FP-PI) simulations that described both the ferroelectric and paraelectric phases[33–36]. Despite these advances, to the best of our knowledge, at present there is neither a fully FP-PI simulation nor an FP-derived model description of the transition to the quantum paraelectric phase under pressure in KDP or DKDP.

FP calculations demonstrated that, due to strong correlations, tunneling in these systems is only allowed through the coherent motion of clusters involving several protons (deuterons) and heavy atoms, with effective masses determined by the contribution of the various atoms to the local tunneling modes[16,17]. Thus, the observed proton double occupancy in the PE phase of KDP should be explained by the tunneling of large and heavy clusters, in addition to thermal fluctuations[17]. This conclusion is supported by the double-site distribution experimentally observed at high pressure and very low T also for the phosphorus atoms[37]. The absence of tunneling in DKDP has been explained in terms of the reduction of the quantum coherence length with increasing mass[26], in turn related to the correlated cluster motion[16,17]. Therefore, the early experimental evidence from neutron diffraction[11,37] suggests the possible onset of a QPE state originating from a pressure-induced delocalization of the correlated cluster[17,26]. This possibility has not yet been demonstrated theoretically, and we will address it here.

We shall develop an effective coarse-grained (CG) model fitted to FP calculations including nonlocal dispersion corrections, vdW-DFT[32]. We then use it to investigate phase transitions under pressure and the associated isotope effects in KDP and DKDP, via path integral Monte Carlo (PIMC) simulations with FP-determined effective masses for H and D, corresponding to the local tunneling modes mentioned above. Our study will address several long-standing issues regarding KDP: (1) the emergence of a quantum paraelectric phase at low temperatures and high pressures; (2) the universal linear correlation between T_c and δ, in connection with the relevance of geometrical effects; (3) the role of the self-consistent mechanism between tunneling and geometric effects in producing the large isotope shift in the FE transition T_c.

II. MODEL AND FIRST-PRINCIPLES CALCULATION DETAILS

A. Local instabilities and FE clusters

The starting point of our description is, as shown by FP calculations, that instabilities in the host PE matrix of KDP-type crystals (modeled with protons fixed at the centers of the O–H$\cdots$O bonds) originate from the correlated motion of several H/D ions along these bonds, accompanied by coherent displacements of K and P atoms[16,17]. In contrast, isolated proton motions are stable and do not lead to distortions. This naturally introduces the concept of *ferroelectric clusters*, defined as minimal structural units of the PE lattice that display local FE-like instabilities when embedded in it. A FE cluster corresponds to a group of H/D and heavy ions that undergo correlated motion through a local double-well potential. One of the smallest such entities involves

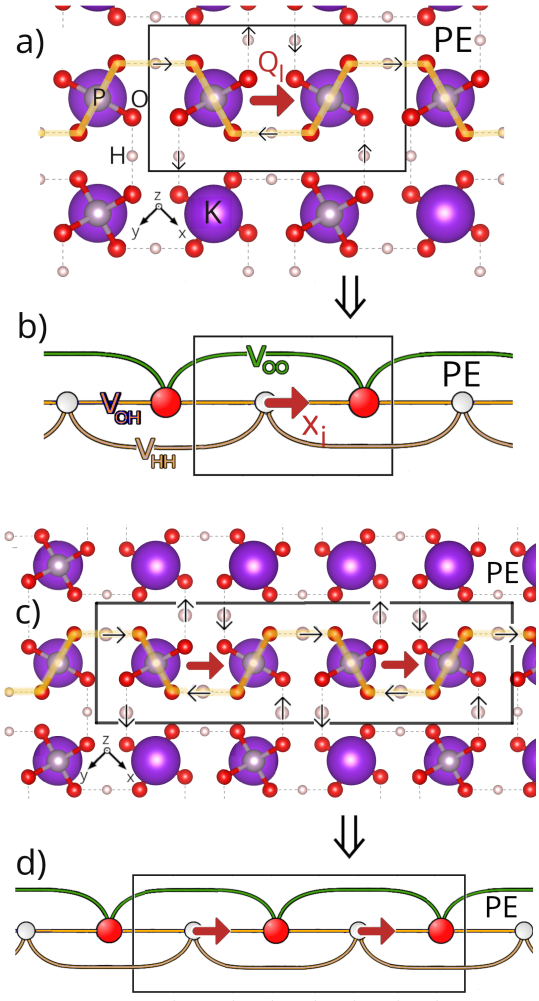

Figure 1. Cluster distortions in the KDP structure and their correspondence to the CG model. a) Schematic representation of a 7 H/D FE cluster (delimited in a rectangular box) embedded in a PE host lattice in KDP. The cluster lies in a chain of H-bonds shown with a yellow bold line. The displacements of the 7 H/D atoms along the FE mode are indicated with black arrows and the collective coordinate Q_l with a red arrow. b) Schematic representation of the CG model in the PE phase composed of concatenated unit cells, one of which is delimited by a rectangle. The unit cell comprises an O ion (red circle) and an effective particle H/D atom (white circle), which interact via V_{OO}, V_{OH}, and V_{HH}, shown as green, orange and gray lines, respectively. We show the $1H_{eff}/1D_{eff}$ distortion (see text) corresponding to the H off-center displacement in the i-th unit cell, x_i (red arrow). This effective distortion in the model is equivalent to the 7 H/D cluster displacement Q_l. c) Same as a) for a 13 H/D cluster. d) Same as b) for two consecutive cells ($2H_{eff}/2D_{eff}$ distortion).

two linked PO_4 groups plus their K ions and seven protons/deuterons. We refer to this as the *7 H/D cluster*, illustrated in Fig. 1a), which in the coarse-grained description corresponds to an effective one-particle displacement (denoted $1H_{eff}$ for protons or $1D_{eff}$ for deuterons) as shown in Fig. 1b). The cooperative displacement of the cluster follows the symmetry of the global FE soft mode. This correlated pattern is represented by a single collective coordinate Q_l (for cluster l) whose value coincides with the H/D off-center displacement x (see the red arrow in Fig. 1a)). For clarity, in the schematic figures of FE clusters we only show H/D displacements, while the coherent motion of the heavy ions is omitted.

Because the heavy ions relax coherently with the H/D displacements, each proton/deuteron behaves as a "dressed particle" with an effective mass larger than the bare proton/deuteron mass. This dressing is crucial, since tunneling of collective clusters is only possible if the effective mass and the local barrier allow quantized levels below the barrier[16,17].

Larger FE clusters can also be considered. A particularly relevant case for the CG model developed below is the *13 H/D cluster*, composed of four linked PO_4 groups plus the corresponding K ions and thirteen protons/deuterons (see Fig. 1c)). Although 13 hydrogens plus corresponding heavy ions are displaced in the FP calculations, the correlated pattern reduces effectively to the motion of only two neighboring hydrogens in the coarse-grained description as shown in Fig. 1d). Thus, while the 7 H/D cluster maps to a single effective degree of freedom ($1H_{eff}$ or $1D_{eff}$), the 13 H/D cluster corresponds to an effective two-particle displacement (denoted $2H_{eff}$ for protons or $2D_{eff}$ for deuterons) (see Figs. 1a-d)). These mappings provide the bridge between the microscopic cluster instabilities and the effective degrees of freedom used in our coarse-grained model.

B. First-principles calculations

To quantify the local energy barriers and effective masses of these clusters, we performed FP calculations using the VASP code[38,39]. The clusters were embedded in a PE supercell ($2 \times 2 \times 2$ primitive cells) containing 16 formula units (128 atoms). We start from the average experimental structure of the PE phase of KDP and DKDP at $T = T_c + 5$ K[40] (space group $I\bar{4}2d$), with the H atoms at the midpoint of the O–H$\cdots$O bonds[17,32]. After ionic relaxation in the PE supercell, we displaced the hydrogen atoms of the 7 or 13 H/D clusters according to the FE soft mode symmetry (see Figs. 1 a) and c)), while allowing relaxation of the P and K ions in the clusters. The chosen supercell size was sufficient to avoid interactions between periodic images of the clusters. We used projector-augmented wave (PAW) all-electron potentials, and the plane-wave basis was expanded to an energy cutoff of 750 eV. An automatic Monkhorst-Pack $5 \times 5 \times 5$ grid sampling of the electronic Brillouin zone proved sufficient to achieve converged results. All atomic relaxations were continued until the forces on every mobile atom were smaller than 5 meV/Å. The exchange-correlation functional used was vdW-DFT, which includes a nonlocal correlation contribution accounting for van der Waals interactions[41–43]. This proved important for a correct de-

scription of the H-bond geometry and energy barriers in KDP[32]. This approach led to a revised, more accurate set of local energy barriers to test our model, and effective masses for use in the PIMC simulations. For the 7 H/D cluster, the revised effective masses of H and D are $\mu_H = 2.7m_p$ and $\mu_D = 3.7m_p$, respectively, where m_p is the bare proton mass.

C. Coarse-grained model

Our coarse grained model is composed of concatenated, effective unit cells, one of which is shown by a rectangle in Fig. 1b), comprising an oxygen ion, and a dressed particle named H/D, characterized by an effective mass (μ_H for protons or μ_D for deuterons), representing the 7 H/D heavy clusters (see Fig. 1a)).

The model includes three types of interactions (Fig. 1b)): O-O, O-H, and H-H interactions. The O-O and O-H interactions are described by the Morse potentials $V_{OO}(R) = D_{OO}\left(1 - e^{-a_{OO}(R-R_0)}\right)^2 - D_{OO}$ and $V_{OH}(q) = D_{OH}\left(1 - e^{-a(q-r_0)}\right)^2 - D_{OH}$, respectively[25,32]. The H-H interaction is taken of the form $V_{HH} = -\frac{1}{2}\sum_{<ij>} J x_i x_j$, where $x_i \equiv \delta_i/2$ is the H off-center displacement in the i-th unit cell. Due to this term, the ice rules arise naturally in the CG model, since correlated neighboring configurations with one proton per oxygen are energetically favored, while those with zero and two protons carry an energy penalty of order J. At finite temperature (or including quantum fluctuations), such higher–energy states may still occur with finite probability, so that thermal and quantum disorder are preserved in the model.

The total potential energy for the CG model, where the V_{HH} interaction is treated in mean field[25], is given by:

$$V_{CGm} = \sum_i \left\{ V_{OH}\left(x_i + \frac{R_i}{2}\right) + V_{OH}\left(\frac{R_i}{2} - x_i\right) \right\} + \sum_i V_{OO}(R_i) - J\langle x\rangle \sum_i x_i + \frac{1}{2} N J \langle x\rangle^2, \quad (1)$$

where R_i is the distance between oxygens in unit cells i and $i+1$, $\langle x\rangle \equiv 1/N \sum_i x_i$ represents the time and lattice average of the H off-centered positions taken at each MC step in the simulation, and N is the total number of unit cells. Treated in mean field, this model exhibits a second-order phase transition at finite T[44].

A key issue is how the model captures the essence of the geometrical effect arising from the real structure. First-principles calculations show that protons centered in the O–H–O bonds in the FE phase act as strong attraction centers that pull the bridging oxygens closer, contracting the lattice[16,17]. Conversely, when atoms relax along the FE mode starting from the PE average structure, the O–O distance and the lattice expands. This behavior reflects the experimentally observed coupling between the FE unstable mode and strain[45,46], also confirmed in FP

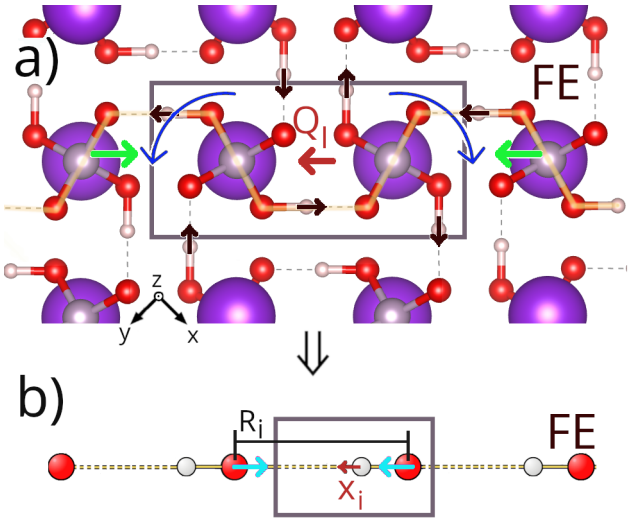

Figure 2. Correlations associated with geometric efects. a) Schematic representation of the FE KDP lattice. A 7 H/D cluster delimited in a rectangular box is shown. The displacements of the 7 H/D atoms along the FE mode are shown with black arrows and the collective coordinate Q_l is shown with a red arrow. Green arrows represent the lattice shrinking when $Q_l \to 0$ (see explanation in text). Blue arrows represent the local PO_4 rotations that couple to the FE mode. b) CG model in the FE phase. Cyan arrows indicate the contraction of R_i as the effective particle H/D moves toward the bond center ($x_i \to 0$, red arrow).

studies of linear $\cdots$F–H$\cdots$F– chains, where it leads to an isotope dependence of the lattice constant[47]. In KDP clusters, the same mechanism appears. For instance, in the FE phase, as $Q_l \to 0$ (see Fig.2a)), protons approach the bond center inducing both a local O–O contraction and cooperative lattice strain (green arrows in Fig.2a)). FP calculations further show that the FE mode strongly couples to a phonon of A_1 symmetry at 543 cm^{-1} (out-of-phase PO_4 librations)[32]. Locally, as $Q_l \to 0$, the FE cluster motion interacts with opposite phosphate rotations in the xy plane (blue curved arrows in Fig.2a)), leading to the O-O distance and lattice contractions.

These couplings are effectively incorporated in the CG model (Fig. 2b)), where the O–O distance R_i acts as a local strain variable coupled to the effective H/D displacement x_i (the $1H_{eff}$ distortion). The anharmonic Morse potentials V_{OO} and V_{OH} ensure the key correlation: decreasing x reduces R, while increasing x enlarges R, which is at the root of the geometrical effect[25,32]. As shown below by PIMC simulations, quantum fluctuations (tunneling) act self-consistently with this correlation[16,17], ultimately producing the observed geometric or Ubbelohde effect[17,47].

In order to study phase transitions in KDP and DKDP, we performed PIMC simulations with the CG potential of Eq. (1), which has seven adjustable parameters. Six of them, i.e. those associated to the O-H and O-O interactions, were fitted using global energy barriers, distances,

and mode frequency data obtained from FP calculations with the vdW-DF functional, as explained in Ref.[32]. The H-H interaction parameter J was adjusted so that the critical temperature of the model with classical nuclei, $T_c^{(cl)}$, (see Fig. 4) matches that obtained by FP molecular dynamics simulations with the vdW-DF functional for DKDP[48], yielding $T_c \approx 350$ K. Details of the fitting procedure can be found in Refs.[25,32]. Model parameters are reported in Table I below.

Table I. Parameters of the CG model

D_{OH}[eV]	a[Å^{-1}]	r_0[Å]	D_{OO}[eV]	a_{OO}[Å^{-1}]	R_0[Å]	J[eV/Å^2]
8.838	3.027	0.966	10.542	0.831	2.917	0.55

D. Validation of the local behavior against FP results

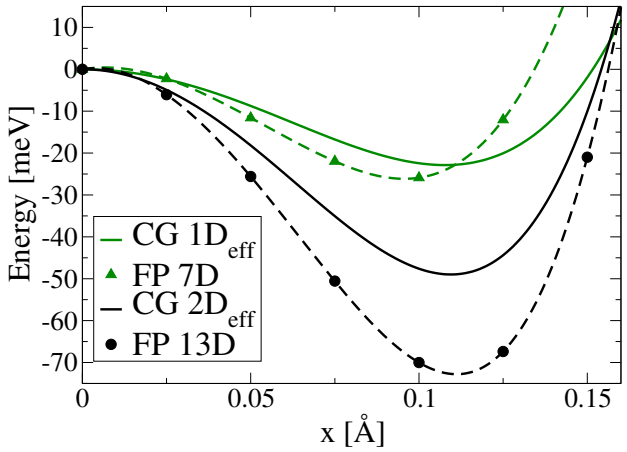

Figure 3. Energy profiles as a function of x for different local cluster distortions embedded in a PE matrix (see text). CG model: solid lines, FP: symbols and dashed lines. In the case of FP, x corresponds to the local coordinate Q for the cluster motion, as defined in text.

Since the model was fitted to global FP energy landscapes, it is important to test its local behavior, which plays a key role in phase transitions. With this aim, we calculated the FP energy profiles of cluster distortions in a PE DKDP matrix and compared them with their CG counterparts. The 7 D cluster distortion corresponds to the 1D$_{eff}$ motion while the 13 D cluster distortion corresponds to the 2D$_{eff}$ motion in the CG model, as explained in Sec. II.A. The energy profiles for these distortions are shown in Fig. 3. The FP energy barrier and minimum for the 7 H/D cluster are well reproduced by the 1D$_{eff}$ motion. For the 13 H/D cluster, the corresponding CG energy barrier for the 2D$_{eff}$ distortion is underestimated by about 28%, although the position of the energy minimum is correctly reproduced. This shows that the CG model captures the essential local physics.

We note that, while the coarse-grained model successfully captures the essential features of the geometrical effect, the local energetics, and the key correlation trends revealed by FP calculations, it has inherent limitations. By construction, it reduces the complex dynamics of protons/deuterons and phosphate groups to effective variables, necessarily neglecting some atomistic details and local fluctuations (e.g., three-dimensional high-energy configurations such as Slater/Takagi defects). The model relies on potential parameters fitted to FP results and focuses on the dominant FE mode coupled to strain and phosphate librations, but it does not explicitly include interactions with other vibrational modes[32,49] or cluster configurations beyond those considered[16,17]. Quantum fluctuations are treated at the level of the effective particle, which reproduces the main isotope effects but cannot capture all subtle correlations present in the full atomic system. Long-range correlations and fluctuations are only approximately accounted for within a mean-field treatment.

The simplicity of the model, however, allows us to undertake a complex calculation of the phase transitions in KDP and DKDP, including both thermal and quantum fluctuations under pressure, which would otherwise be prohibitively expensive if all degrees of freedom were treated at the FP level (i.e., an all-atom full quantum FP simulation of the phase transition). We will show below that the simple CG model developed here is capable of describing the isotope effects on T_c and the order parameter, the pressure effects, the linear correlation between T_c and δ, and, moreover, the emergence of a QPE phase at high pressure and low temperature.

E. Path Integral Monte Carlo simulations

In the PIMC simulations, the effective short-time propagator is evaluated to fourth-order accuracy with the Takahashi-Imada approximation, allowing us to reduce the Trotter number M to 128 beads for the quantum polymer of each atom, yielding converged results. For D at 18.7 kbar and $T \leq 60$K, we needed 256 beads for convergence. A normal-mode representation of the quantum polymers was used to ensure ergodicity in the MC sampling[50]. We performed 3×10^4 thermalization steps followed by 10^5 MC steps for computing averages. Each result was obtained from an average of 20 runs with different random number generator seeds. During the simulations all x_i and R_i were allowed to vary in each unit cell i. The simulations were conducted in an NPT ensemble where the supercell size L was relaxed at constant stress σ, except for the fixed cell simulations where the oxygens were fixed. The supercell was subjected to periodic boundary conditions and contained $N=$ 200 unit cells, which proved sufficient for the convergence of phase-transition properties. To compare with experiments, the applied stress σ in the model was related to an equivalent hydrostatic pressure

p in the lattice, using an equivalence of 1 eV/Å $\approx$ 62.3 kbar, an estimate based on the pressure-dependent density of H-bond chains per unit area in the KDP lattice.

The quantum behavior of each particle was studied by analyzing the centroid X_{CM} and the radius of gyration R_g of the quantum polymer[34,51]. The centroid is defined as the center of mass (CM) of the polymer $X_{CM} \equiv M^{-1} \sum_{s=1}^{M} x_s$, giving the average position of the quantum particle. The index s runs over time slices in the polymer and x_s is the particle position for the corresponding bead. On the other hand, the radius of gyration is defined as $R_g \equiv \left(M^{-1} \sum_{s=1}^{M} |x_s - X_{CM}|^2 \right)^{1/2}$, and represents the spread of the quantum path. It measures how far the beads or monomers are from the polymer center, providing information on the quantum delocalization of the particle, a quantity that increases during tunneling[34,51]. For a free particle, for instance, its value is proportional to the thermal wavelength.

III. RESULTS AND DISCUSSION

A. Isotope effects on T_c and the order parameter

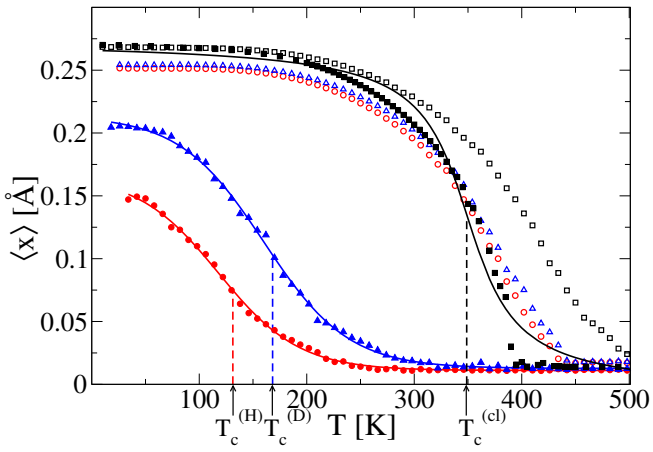

Figure 4. PIMC off-centering order parameter $\langle x \rangle$ as a function of T. Classical nuclei (solid black squares and line); quantum D (solid blue triangles and line); quantum H (solid red circles and line). Corresponding open symbols are the results for fixed cell simulations. Estimated transition temperatures are marked by vertical dashed lines. The smearing is due to finite size.

The PIMC results for the averaged order parameter $\langle x \rangle$ (H off-centering) as a function of T are plotted in Fig. 4. Beyond the smearing, caused by our finite size, one can infer second-order phase transitions in all cases, where $\langle x \rangle$ decreases from a saturated value at low T to negligible values at high T. Arbitrarily, but reasonably, we define T_c as the temperature corresponding to the semisum of both limiting values. We note here that the uncertainties introduced by limited size impede possible inquiries about critical behaviour and quantum/classical crossover. The classical nuclei case ($M = 1$ in the PIMC calculations, which is equivalent to classical Monte Carlo) shows a $T_c^{cl} \approx 350$ K, which drops dramatically when quantum corrections are included to $T_c^D \approx 170$ K and $T_c^H \approx 130$ K for DKDP and KDP, respectively, as shown in Fig. 4. T_c^H is in very good agreement with experiments, while T_c^D is underestimated by a 25% which is reasonable in view of the simplicity of the model. Specifically, the larger energy and length scales of DKDP[17], combined with the omission of interactions between the FE and other modes[32,49], may explain the underestimation of effective interactions (see Fig. 3) and hence the discrepancy in T_c^D. Nevertheless, a large isotope effect of ≈ 40 K is found, in fair agreement with experiments. Moreover, the nearly saturated value of the order parameter $\langle x \rangle$ at low $T \approx 40$ K shows an isotope effect of $\approx 33\%$ (see Fig. 4), which agrees reasonably well with experiment[40] ($\approx 23\%$) Furthermore, the isotope effect in the O-O distance at low T is $\approx 1.04\%$ in fair agreement with experiment[40] ($\approx 1.44\%$). Hence, the geometric effect is reproduced to a good extent by our simulations. This contrasts with the fixed cell results, where the isotope effects in T_c and the order parameter $\langle x \rangle$ are negligible (see open triangles and circles in Fig. 4), thus confirming that the interplay between FE mode and strain is crucial. Tunneling alone in a fixed lattice potential (fixed oxygens) is not able to account for the large isotope effect in the system. However, by relaxing the oxygens in the simulations, the selfconsistent mechanism between tunneling and H-bond geometry[16,17] is turned on, leading to the large isotope effect observed.

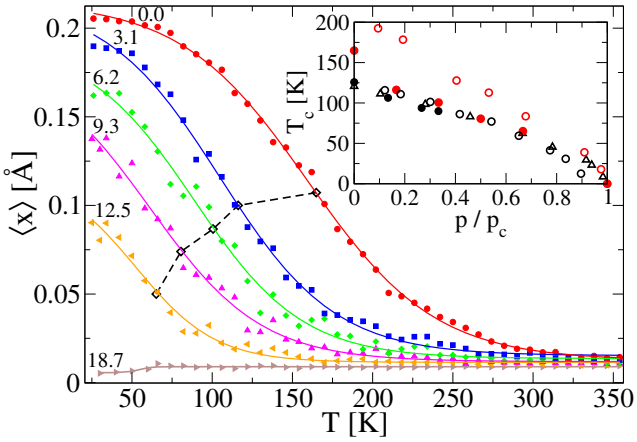

Figure 5. Off-centering order parameter $\langle x \rangle$ as a function of T for DKDP at increasing pressure p marked near each curve (units are kbar). Open diamonds denote the values of T_c. The inset shows T_c as a function of the normalized pressure p/p_c for the model (solid circles) and the experiments of Ref.[52] (open triangles) and Refs.[53,54] (open circles), for KDP (black) and DKDP (red).

B. Pressure effects and the T_c-δ linear correlation

Now we turn to pressure effects. In Fig. 5, we plot $\langle x \rangle$ as a function of T for different p. The results show that $\langle x \rangle$ and T_c decrease as p increases. Moreover, in Fig. 7, the calculated particle probability distributions (PPD) for the coordinates R and x at $T = 50$ K indicate that these distributions become more symmetric around $x = 0$ as p increases for both H and D. This behavior reflects the suppression of ferroelectric order with increasing pressure, consistent with the observed drop in T_c shown in Fig. 5. In the inset to the latter we show that the decreasing rate of T_c with p for the model agrees with experiments for KDP and is underestimated for DKDP.

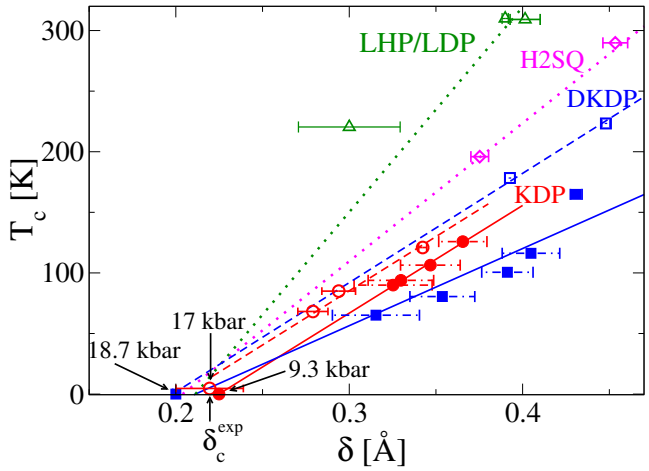

Figure 6. T_c as a function of δ. Red solid circles (blue solid squares) show model results for KDP (DKDP), while red open circles and dashed lines (blue open squares and dashed lines) show experimental data from Ref.[11]. Red (blue) solid lines: linear regressions of the model results for KDP (DKDP). Also shown are experimental data[11] for LHP/LDP [H2SQ] (green [magenta] open triangles [diamonds] and dotted lines), and theoretical (statistical) and experimental error bars for δ. Dashed and dotted lines are linear extrapolations reproduced from Ref.[11]. Additional experimental data at ambient pressure for LDP and H2SQ, not displayed for clarity since they fall outside the chosen scale, also support the linear scaling of T_c with δ[11].

Encouraged by these results, we analyzed the specific importance of geometric effects due to quantum fluctuations in the model. To this end, we related, for each p, the calculated T_c with the value δ corresponding to the distance between peaks, or $2x_p$, in the probability distribution at T_c . In Fig. 6 we plot T_c vs. δ for both H and D and compare the results with the experimental data of Ref.[11]. In agreement with experiments and recent all-atom path integral molecular dynamics (PIMD) calculations[36], we find a linear correlation between T_c and δ. In particular, the slope of the linear curve agrees remarkably well with that from experiments in the KDP case, although it is underestimated in the deuterated case. Also in agreement with the experiment

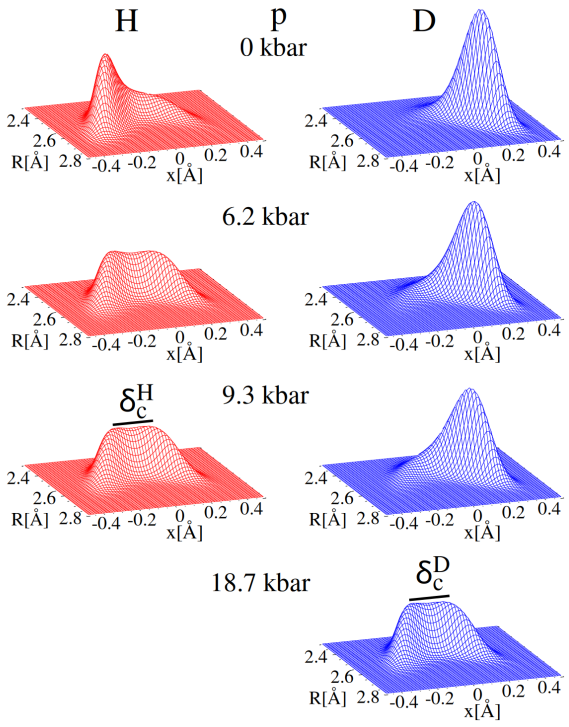

Figure 7. Particle probability distributions (PPD) of the H-bond variables R and x at $T = 50$K and different pressures for H and D.

is the critical value $\delta_c^H \approx 0.22$Å, at which T_c vanishes for KDP, signaling a "quantum" PE (QPE) state, as will be shown below. The critical p that leads to the QPE phase is $p_c^H \approx 9.3$ kbar, which compares not indecently with experiments (≈ 17 kbar), taking into account the simplicity of our model. For DKDP, we find quantum paraelectricity at $p_c^D \approx 18.7$ kbar with $\delta_c^D \approx 0.2$Å, actually in agreement with the critical value extrapolated from the experimental linear curve shown in Fig. 6. It is worth noting that theoretical H and D linear curves can be rearranged to almost coincide in one line for both cases within statistical error bars, similarly to what occurs experimentally (see Fig. 6). This is an important feature, which was also highlighted in Ref.[11], indicating that the relevant geometrical parameter that defines T_c is δ, independently of the mass of the tunneling particle. Moreover, as shown in the PPD results of Fig. 7, the bimodal distributions for H at 9.3 kbar and for D at 18.7 kbar are almost identical. In other words, the effect of deuteration can be reverted by applying pressure, demonstrating once more the significance of geometric effects.

C. The quantum paraelectric phase

In order to further analyze the quantum nature of the PE states found at critical pressures p_c^H and p_c^D, in Fig.

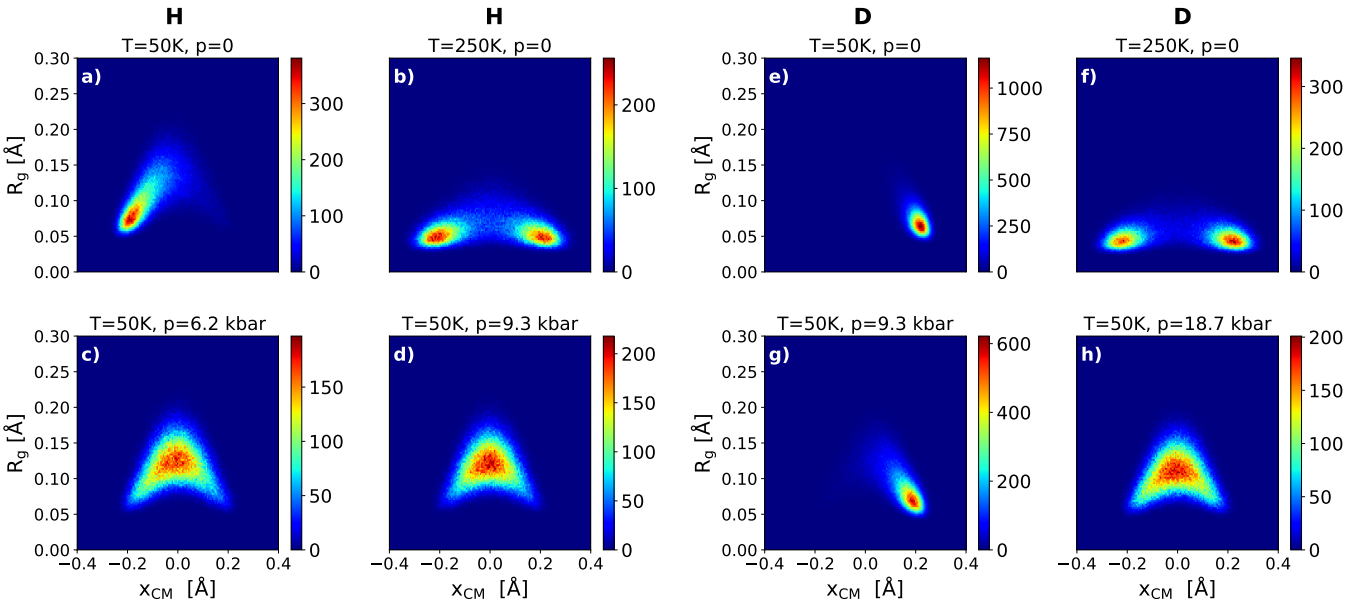

Figure 8. Probability distributions of the radius of gyration R_g for the quantum polymers as a function of the mass-center coordinate X_{CM}, for different temperatures and pressures indicated in each panel. The four panels to the left (a-d) correspond to H, while the four ones to the right (e-h) are for D. The intensity for the histograms in each panel has arbitrary units.

8 we plot the probability distribution of R_g for the quantum polymers vs. the center-of-mass coordinate X_{CM} for different cases. First, we focus on the zero pressure case (see the top panels in the Figure). At T=50K, the deuteron (Fig. 8e)) shows a well defined peak at $R_g \approx 0.05$Å and $X_{CM} \approx 0.2$Å, indicating that here D behaves classically ($R_g < \delta$) and is localized in one of the energy minima of the bond. This is consistent with the corresponding single peak for the PPD of D in the FE phase, as shown in Fig. 7. The situation changes for H (Fig. 8a)), which shows an asymmetric R_g distribution with respect to X_{CM}. It has a peak at $X_{CM} \approx$ -0.2Å, which is equivalent to that of D but centered in the opposite minimum of the symmetric well. However, it also displays a significant weight around the H-bond center ($X_{CM} = 0$) and even some weight on the other side of the H-bond (positive values of X_{CM}). At $X_{CM} = 0$, R_g takes values as high as 0.19Å signaling quantum delocalization over the local energy barrier ($R_g \approx \delta$) and the strong effect of quantum tunneling. This explains the asymmetric PPD observed for H in the FE phase at T=50K and zero pressure (see Fig. 7). Therefore, we can conclude that at zero pressure in the FE case, tunneling is allowed for H but is essentially absent for D. Similarly, an increase of R_g as $X_{CM} \to 0$ was reported in first-principles PIMD simulations of squaric acid, where it was linked to collective proton tunneling along the H-bond network[34].

At zero pressure and T=250K, both H and D are in the thermal PE phase with vanishing order parameter (see Fig. 4). In these cases, we see in Figs. 8b) and f), double-peak distributions for the X_{CM} variables, consistent with the proton/deuteron double-site distribution observed in the disordered PE phase by neutron diffraction[11], and with the double-peak distribution found for D in all-atom FP PIMD simulations[33], although inconclusive results were reported for H in the same study. Moreover, in our effective model, and due to strong correlations in the real system, the motion of the dressed particle (cluster motion) represents also that of the heavy ions involved in the local FE mode (see Fig. 1a)). Hence, our results of double occupancy are in agreement with the experimental evidence of a double-site distribution of the P atoms in the PE phase at room pressure[37,55]. In the deuteron case, R_g remains practically below 0.07Å showing a classical behavior ($R_g < \delta$) with no clear sign of tunneling. Thus, the double-occupancy for D in the PE phase is originated mainly from thermal fluctuations. For H, however, R_g increases to values as high as $\approx$ 0.13Å , indicating the presence of tunneling, in addition to thermal disorder. Overall, we find at zero pressure, for both phases, that D behaves classically (no clear sign of tunneling) whereas H shows indications of tunneling and particle delocalization towards the middle of the H-bonds. This explains the behavior observed in Compton scattering experiments[26,27]. On the other hand, Figs. 8b) and f) show an increase with deuteration of the distance between peaks along the X_{CM}-axis, namely $\delta = 2x_p = 2X^p_{CM}$, where X^p_{CM} is the corresponding peak-position coordinate. We find for H at 250K and room pressure that $\delta^H \approx 0.381$Å which increases to $\delta^D \approx 0.435$Å with deuteration. These values are in good agreement with the corresponding experimental data for δ in the PE phase at $T_c + 5K$: 0.343Å for KDP and 0.448Å for DKDP[40]. Thus, our calculations show that the geometrical effect is also fulfilled at high

temperature in the PE phase.

In the case of H at T=50K with an applied pressure of 6.2 kbar, simulations reveal that tunneling is greatly enhanced with respect to the zero pressure case (compare Figs. 8a) and c)) The peak of the R_g-distribution shifts to the middle of the H-bond and is spread around 0.14Å, indicating a large quantum delocalization of the particles. Moreover, R_g reaches values as high as 0.20Å, as shown in Fig. 8c). However, at $p = 6.2$ kbar, the PPD for H shows a slight asymmetry (see Fig. 7), indicating that the system is still in the FE phase. Increasing further the pressure to $p_c^H = 9.3$ kbar, tunneling further dominates the scene as shown in Fig. 8d), but now the PPD becomes completely symmetrical in x and the system transitions to a QPE state with a double-peak distribution in x (see Fig. 7). The quantum character of the PE phase can additionally be visualized in the behavior of the R_g-distribution in Fig. 8d), which shows, around the middle of the H-bond, a large weight of values of R_g between 0.10 and 0.17Å, reaching also higher values of the order of δ_c^H. This underlines how quantum delocalization and tunneling prevail in this case.

For D at $p = 9.3$ kbar and T=50K (Fig. 8g)), the R_g-distribution shows some weight spread to the middle of the H-bond, where R_g reaches values as high as 0.15Å, indicating quantum delocalization, as opposed to the classical behavior of the zero pressure case –compare Figs. 8e) and 8g). Thus, at p =9.3 kbar, the deuteron too can tunnel and spend some time on the other side of the bond, which is reflected in the asymmetric PPD (see Fig. 7). The system still remains in the FE phase at this pressure.

By increasing p for D, we observe at $p = p_c^D$ =18.7 kbar and T=50K (Fig. 8h)) that the R_g-distribution becomes symmetric respect to X_{CM} with most of the weight towards the middle of the bond and with R_g reaching values as high as $\approx \delta_c^D$. This indicates quantum delocalization and tunneling. Moreover, the corresponding PPD (see Fig. 7) shows a symmetric distribution along x indicating that the system is in the PE phase (the order parameter vanishes, as shown in Fig. 5). As quantum tunneling is predominant, we conclude that the system achieves a QPE phase at this critical pressure, in contrast to the classical PE phase at 250K, which exhibits a very different, two-site distribution (see Fig. 8f)).

By comparing Figs. 8d) and h), which correspond to the QPE phases found for H and D, respectively, we see that the corresponding R_g-distributions are strikingly similar. This is in remarkable correspondence with alike PPDs obtained for H and D at 9.3 kbar and 18.7 kbar, respectively, as shown in Fig. 7. Moreover, for these distributions, we have found $\delta_c^H \approx \delta_c^D$, which are indeed very close to the experimental critical value $\delta_c \approx 0.22$ Å[11] (see also Fig. 6). Overall, these observations enable us to conclude that, in our simulations, quantum paraelectricity emerges under pressure for both, H and D, albeit at different pressures. The QPE states are remarkably similar thus showing isotopic independence, which is also reflected in a unique or universal value of δ_c, in agreement with neutron diffraction experiments[11]. In our CG model, the QPE states found are originated in the quantum delocalization of correlated clusters for the H and D motion which may explain the order-disorder behavior observed for the P atoms at very low T and high p[37].

IV. CONCLUSIONS

In summary, our PIMC simulations described isotope and in particular high pressure effects on the KDP FE-PE transition using a simple model fitted to FP calculations including nonlocal vdW corrections. The results confirm that the large isotope effect in the T_c stems from a strong nonlinear feedback between tunneling and off-center H-bond geometric effects[16,17]. This amplification mechanism leads to the dominance of geometric effects, further supported by the linear correlation found between T_c and δ, in agreement with experiments[11,23]. The geometric significance, as also reflected by volume, is also demonstrated by analyzing PPDs at different pressures, where we have shown that the effect of deuteration can be reverted by applying pressure. The analysis of the radius of gyration of the quantum polymers confirms that quantum PE phases emerge above a critical pressure where R_g-distributions and PPDs are remarkably similar (e.g., $\delta_c^H \approx \delta_c^D$, see Fig. 7), regardless of tunneling masses. This could explain the universality of δ_c observed in protonated and deuterated compounds[11]. Moreover, this universality spans various chemical environments and H-bond network dimensionalities[11] (see Fig. 6) and, as δ_c seems rooted in a local "dressed" H-bond feature, we propose that CG models adequately parameterized for other H-bonded FE and Anti-FE compounds would reproduce this universal behavior.

ACKNOWLEDGMENTS

We would like to dedicate this paper to Ricardo Migoni who, in the early 80s, created the ferroelectricity research group at Instituto de Física Rosario (IFIR). Through Ricardo's guidance and generous mentoring, this group became an important actor in the field and has blossomed and branched into several directions. The present paper rounds up a body of research in H-bonded ferroelectrics, pioneered by Ricardo as an Associate member of ICTP, in collaboration with four co-authors of this paper. We are particularly indebted to Charusita Chakravarty, a brilliant researcher and fascinating human being, who sadly left us too early. In this paper we used her PIMC simulation method as inspiration. ET would also like to dedicate this paper to Annabella Selloni, who was his first student, a lifelong friend and wonderful colleague, on the occasion of her retirement from Princeton University. Last but not least, we thank Michele Parrinello for his countless contributions to the field of computer sim-

ulation, many of which are, directly or indirectly, used in this research.

DATA AVAILABILITY

The data that support the findings of this study are available from the corresponding author upon reasonable request.

REFERENCES

[1]K. A. Müller and H. Burkard, Phys. Rev. B **19**, 3593 (1979).
[2]K. A. Müller, W. Berlinger, and E. Tosatti, Z. Phys. B **84**, 277 (1991).
[3]S.Hameed, D. Pelc, Z. W. Anderson, A. Klein, R. J. Spieker, L. Yue, B. Das, J. Ramberger, M. Lukas, Y. Liu, M. J. Krogstad, R. Osborn, Y. Li, C. Leighton, R. M. Fernandes, and M. Greven, Nat. Mater. **21**, 54 (2022).
[4]A. Narayan, A. Cano, A. V. Balatsky, and N. A. Spaldin, Nat. Mater. **18**, 223 (2019).
[5]K. Dunnett, J.-X. Zhuand, N. A. Spaldin, V. Juričić, and A. V. Balatsky, Pys. Rev. Lett. **122**, 057208 (2019).
[6]P. Chandra, G. G. Lonzarich, S. E. Rowley, and J. F. Scott, Rep. Prog. Phys. **80**, 112502 (2017).
[7]D. Shin, S. Latini, C. Schäfer, S. A. Sato, U. D. Giovannini, H. Hübener, and A. Rubio, Phys. Rev. B. **104**, L060103 (2021).
[8]S. E. Rowley, L. J. Spalek, R. P. Smith, M. P. M. Dean, M. Itoh, J. F. Scott, G. G. Lonzarich, and S. S. Saxena, Nat. Phys. **10**, 367 (2014).
[9]H. P. Soon, H. Taniguchi, and M. Itoh, Appl. Phys. Lett. **95**, 242904 (2009).
[10]X. Li, T. Qiu, J. Zhang, E. Baldini, J. Lu, A. M. Rappe, and K. A. Nelson, Science **364**, 1079 (2019).
[11]R. J. Nelmes, M. I. McMahon, R. O. Piltz, and N. G. Wright, Ferroelectrics **124**, 355 (1991).
[12]Y. Moritomo, Y. Tokura, H. Takahashi, and N. Mori, Phys. Rev. Lett. **67**, 2041 (1991).
[13]S. Endo, K. Deguchi, and M. Tokunaga, Phys. Rev. Lett. **88**, 035503 (2002).
[14]S. P. Dolin, A. A. Levin, T. Y. Mikhailova, M. V. Solin, N. S. Strokach, and N. I. Kirillova, Int. J. Quantum Chem. **96**, 247 (2004).
[15]S. Horiuchi and S. Ishibashi, J. Phys. Soc. Jpn. **89**, 051009 (2020).
[16]S. Koval, J. Kohanoff, R. L. Migoni, and E. Tosatti, Phys. Rev. Lett. **89**, 187602 (2002).
[17]S. Koval, J. Kohanoff, J. Lasave, G. Colizzi, and R. L. Migoni, Phys. Rev. B **71**, 184102 (2005).
[18]M. E. Lines and A. M. Glass, Principles and applications of ferroelectrics and related materials (Clarendon Press, Oxford, 1977).
[19]G. A. Samara, Ferroelectrics **71**, 161 (1987).
[20]A. Katrusiak, Ferroelectrics **188**, 5 (1996).
[21]S. Koval, J. Lasave, R. L. Migoni, J. Kohanoff, and N. S. Dalal, "Ab initio studies of h-bonded systems: The cases of ferroelectric KH_2PO_4 and antiferroelectric $NH_4H_2PO_4$," in Ferroelectrics – Characterization and Modeling, edited by M. Lallart (InTech, 2011) Chap. 21, pp. 411–436.
[22]R. Blinc, J. Phys. Chem. Solids **13**, 204 (1960).
[23]M. I. McMahon, R. J. Nelmes, W. F. Kuhst, R. Dorwarth, R. O. Piltz, and Z. Tun, Nature **348**, 317 (1990).
[24]J. M. Robertson and A. R. Ubbelohde, Proc. R. Soc. London A **170**, 222 (1939).
[25]F. Torresi, J. Lasave, and S. Koval, Condens. Matter Phys. **25**, 43708 (2022).
[26]G. F. Reiter, A. Shukla, P. Platzman, and J. Mayers, New J. Phys. **10**, 013016 (2002).
[27]G. F. Reiter, J. Mayers, and P. Platzman, Phys. Rev. Let. **89**, 135505 (2002).
[28]N. Kojyo and Y. Onodera, J. Phys. Soc. Jpn. **57**, 4391 (1988).
[29]H. Sugimoto and S. Ikeda, Phys. Rev. Lett. **67**, 1306 (1991).
[30]A. Bussmann-Holder and K. H. Michel, Phys. Rev. Lett. **80**, 2173 (1998).
[31]D. Merunka and B. Rakvin, Phys. Rev. B **66**, 174101 (2002).
[32]R. Menchón, G. Colizzi, C. Johnston, F. Torresi, J. Lasave, S. Koval, J. Kohanoff, and R. Migoni, Phys. Rev. B **98**, 104108 (2018).
[33]V. Srinivasan and D. Sebastiani, J. Phys. Chem. C **115**, 12631 (2011).
[34]K. T. Wikfeldt and A. Michaelides, J. Chem. Phys. **140**, 041103 (2014).
[35]E. A. Engel, J. Chem. Phys. **148**, 144708 (2018).
[36]B. Yang, P. Xie, and R. Car, npj Comput. Mater. **10**, 241 (2024).
[37]M. I. McMahon, R. J. Nelmes, R. O. Piltz, W. F. Kuhs, and N. G. Wright, Ferroelectrics **124**, 351 (1991).
[38]G. Kresse and J. Furthmüller, Comput. Mater. Sci. **6**, 15 (1996).
[39]G. Kresse and J. Furthmüller, Phys. Rev. B **54**, 11169 (1996).
[40]R. J. Nelmes, Z. Tun, and W. F. Kuhs, Ferroelectrics **71**, 125 (1987).
[41]M. Dion, H. Rydberg, E. Schröder, D. C. Langreth, and B. I. Lundqvist, Phys. Rev. Lett. **92**, 246401 (2004).
[42]J. Klimeš, D. R. Bowler, and A. Michaelides, Phys. Rev. B **83**, 195131 (2011).
[43]G. Román-Pérez and J. M. Soler, Phys. Rev. Lett. **103**, 096102 (2009).
[44]T. R. Koehler and N. S. Gillis, Phys. Rev. B **13**, 4183 (1976).
[45]E. M. Brody and H. Z. Cummins, Phys. Rev. Lett. **21**, 1263 (1968).
[46]R. L. Reese, I. J. Fritz, and H. Cummins, Phys. Rev. B **7**, 4165 (1973).
[47]I. Scivetti, N. Gidopoulos, and J. Kohanoff, Phys. Rev. B **78**, 224108 (2008).
[48]R. Menchón, F. Torresi, J. Lasave, and S. Koval, Condens. Matter Phys. **25**, 43709 (2022).
[49]G. Colizzi, J. Kohanoff, J. Lasave, and R. L. Migoni, Ferroelectrics **401**, 200 (2010).
[50]C. Chakravarty, Int. Rev. Phys. Chem. **16**, 421 (1997).
[51]J. A. Morrone, L. Lin, and R. Car, J. Chem. Phys. **130**, 204511 (2009).
[52]G. A. Samara, Ferroelectrics **7**, 221 (1974).
[53]S. Endo, T. Sawada, T. Tsukawake, Y. Kobayashi, M. Ishizuka, K. Deguchi, and M. Tokunaga, Solid State Commun. **112**, 655 (1999).
[54]S. Endo, K. Deguchi, and M. Tokunaga, J. Phys.: Condens. Matter **14**, 11275 (2002).
[55]M. I. McMahon, R. J. Nelmes, R. O. Piltz, and W. F. Kuhs, Europhys. Lett. **13**, 143 (1990).